JPhys Materials

PAPER • **OPEN ACCESS**

An in-depth study of the synthesis of $ReSe_2$ for anisotropic Raman characteristics

To cite this article: Giho Nam *et al* 2024 *J. Phys. Mater.* **7** 045005

Journal of Physics: Materials

PAPER

An in-depth study of the synthesis of $ReSe_2$ for anisotropic Raman characteristics

Giho Nam[1], Sohyeon Park[1], Keun Heo[1], Jungwoo Bong[1], DongGyu Lee[1], Hyunsoo Kim[1], Krishna Moorthy Ponnusamy[1], Hagyoul Bae[2], Hyeong Gi Park[3,*], Jae-Hyun Lee[4,*] and Hyeon-Sik Jang[1,*]

[1] Semiconductor Physics Research Center, School of Semiconductor Science and Technology, Jeonbuk National University, Jeonju 54896, Republic of Korea
[2] Department of Electronics Engineering, Jeonbuk National University, Jeonju-si 54896, Republic of Korea
[3] AI-Superconvergence KIURI Translational Research Center, Ajou University, Suwon 16499, Republic of Korea
[4] Department of Materials Science and Engineering and Energy Systems Research, Ajou University, Suwon 16499, Republic of Korea
* Authors to whom any correspondence should be addressed.

E-mail: hgpark007@ajou.ac.kr, jaehyunlee@ajou.ac.kr and hsjang88@jbnu.ac.kr

Keywords: $ReSe_2$, chemical vapor deposition, tilted boat, Raman spectroscopy, anisotropic

Supplementary material for this article is available online

OPEN ACCESS

RECEIVED
14 December 2023

REVISED
26 May 2024

ACCEPTED FOR PUBLICATION
26 September 2024

PUBLISHED
8 October 2024

Abstract

Two-dimensional transition metal dichalcogenides (TMDs) have received more interest for their potential role in future electronic and optoelectronic applications. Unlike other TMDs, Rhenium diselenide ($ReSe_2$) stands out for its distinctive anisotropic growth characteristics. These unique features arise from its low lattice symmetry and interlayer decoupling, this has sparked significant interest among researchers. Previous research has indicated the presence of various growth patterns, including dendritic formations and structures resembling flowers. In this study, we effectively produced $ReSe_2$ using the 'Tilting Boat' method to achieve growth on a 21 μm scale. Through precise manipulation of the growth conditions, we successfully attained flakes of 21 μm scale in comparison to prior findings. Moreover, we successfully produced a variety of shapes, including triangles, diamonds, and hexagons, on 1 $\times$ 1 cm^2 Si/SiO_2 substrates. Furthermore, we achieved the successful production of a continuous $ReSe_2$ film on a 1 $\times$ 3 cm^2 Al_2O_3 substrate. We verified the distinct anisotropic properties of $ReSe_2$ via Raman Spectroscopy. Furthermore, we acquired three-dimensional visual representations of $ReSe_2$ flakes and continuous films via SEM measurements. By employing EDS data and analysing x-ray photoelectron spectroscopy spectra, we have established a compositional ratio of 1:2 for Re and Se, which aligns with the MX_2 structure. This confirmation indicates the successful synthesis of high-quality $ReSe_2$ flakes.

1. Introduction

Two-dimensional (2D) transition metal dichalcogenides (TMDs) materials exhibit an MX_2 structure, characterized by one transition metal atom sandwiched between two chalcogen atoms in a layered arrangement, held together by relatively weak van der Waals forces [1, 2]. Generally, 2D nanosheets exhibit distinct physical properties compared to its bulk counterparts. Indeed, materials like MoS_2, WS_2, and WSe_2 are well-known 2D materials that have gained significant attention in the scientific and engineering communities for their unique properties and versatility in various device applications [3–9]. Nevertheless, rhenium diselenide ($ReSe_2$) stands out from other TMDs thanks to its optical characteristics and anisotropy, making it more attractive [10–13]. The bandgap of monolayers $ReSe_2$ is 1.1 eV, while for multilayers is 1.3 eV [14, 15]. Typically, $ReSe_2$ exhibits a triclinic atomic structure with a lattice constant of $a = 3.32$ Å [16]. One intriguing aspect of $ReSe_2$ is its ability to maintain consistent bandgap properties regardless of variations in thickness. Even in the face of challenges associated with achieving precise thickness control, $ReSe_2$ exhibits similar performance, making it a promising candidate for applications in photodetectors and

next-generation devices [2, 17–20]. In specific, the element Re exhibits anisotropic properties due to its diamond chain-like structure, leading to the splitting of energy levels when exposed to linearly polarized light. This attribute finds practical application in image sensors since its behavior changes based on the direction of incident light polarization [3–9]. The significant expansion of TMD material research has been driven by the miniaturization of devices, particularly focusing on group VI TMDs like MoS_2 and $MoSe_2$ [21–25]. Nevertheless, further investigation is required to address the synthesis of group VII transition metals such as Re, with existing methods for $ReSe_2$ synthesis proving to be challenging at a larger scale. Consequently, current research predominantly relies on mechanical exfoliation methods, and there is limited prior exploration of alternative synthesis techniques. Despite $ReSe_2$ demonstrating relatively stable bandgap characteristics across different layer numbers, the attainment of superior electrical properties necessitates the synthesis of $ReSe_2$ with fewer layers and larger surface areas. There are various methods for synthesizing $ReSe_2$, including the chemical vapor transport Reactions method [18, 26], where solid-state precursors transport elements or compounds to synthesize, and the Bridgman method [14], which crystallizes liquid-state precursors at high temperatures to form single crystals. It is important to note that these methods result in doped materials that are transport agent dependent [14]. Furthermore, they are synthesised as 3D bulk crystals [14, 26], which requires a mechanical exfoliation process. Unlike other 2D materials, anisotropic 2D materials such as $ReSe_2$ have the disadvantage that they are easily broken during the exfoliation process due to their orientation-dependent mechanical properties [27, 28]. In this study, we employed the chemical vapor reaction method, which is a bottom–up approach suitable for large-area synthesis of 2D materials. chemical vapor deposition (CVD) process is a technical method where gaseous chemical precursors undergo chemical reactions on a solid surface to form thin films. In this process, the gaseous precursors participate in reactions and deposit as solids. Typically, the CVD process involves several steps: precursor supply, surface adsorption, chemical reaction, deposition and growth, and finishing. The precursors are supplied into the system and exist in the gas phase, then they adsorb onto the solid surface. There, chemical reactions take place, and the resulting material is deposited on the surface to form a thin film. The formed thin film undergoes appropriate post-treatment processes for finishing. Therefore, faster synthesis over a larger area was achieved compared to conventional methods.

The aim of this study is to make a meaningful contribution to the large-scale synthesis of $ReSe_2$ for potential applications in next-generation devices. To achieve this, we performed processes utilizing atmospheric pressure CVD (APCVD) and low pressure CVD (LPCVD) within a quartz tube with diameter of 3 cm and a length of 225 cm. We confirmed the formation of $ReSe_2$ flakes and successful synthesis of $ReSe_2$ films using the tilted substrate. We believe that our research has established a significant groundwork for the investigation of group VII TMDs by acquiring essential data regarding the synthesis of $ReSe_2$. We anticipate that these advancements will lead to superior optical properties and electrical characteristics, thereby significantly enhancing the performance of next-generation devices.

2. Methods

2.1. Preparation

We synthesized two types of $ReSe_2$ using AP/LPCVD with a graphite boat. The growth was performed in a quartz tube with a diameter of 3 cm and a length of 225 cm, which was cleaned with flushing H_2 for 10 min. Additionally, prior to the growth process, the boat was thoroughly rinsed with isopropyl alcohol.

2.2. $ReSe_2$ flake growth on SiO_2 substrate

Firstly, for $ReSe_2$ flake formation, we employed a 1×1 cm^2 Si/SiO_2 substrate. The recipe involved using ReO_3 30 mg (Alfa Aesar, purity 99.9%) and Se 60 mg (Alfa Aesar, purity 99.9%) as precursors, with Ar (75 sccm) serving as carrier gas. **In** figure 1 CVD schematic, the zone 1 from the left, measured from the heating zone, was set to 760 °C without any material placed. ReO_3 was positioned in the zone 2, with a process temperature of 560 °C, and the zone 3 was set to 320 °C, with the temperature ramping up over 5 min. The process was carried out at atmospheric pressure, 760 Torr, and lasted for 20 min. For film $ReSe_2$ synthesis, we used a ReO_3 7 mg (Alfa Aesar, purity 99.9%) and Se 100 mg (Alfa Aesar, purity 99.9%) recipe with Ar (60 sccm) and H_2 (10 sccm) as precursors and carrier gases. In figure 1 CVD schematic, the third zone from the left was set to 760 °C without any material placed, ReO_3 was placed in the second zone, with a process temperature of 750 °C, and the third zone was set to 250 °C, with the temperature ramping up over 15 min. The process was conducted at 1 Torr of pressure and lasted for 30 min.

2.3. $ReSe_2$ film growth on Al_2O_3 substrate

We used a 1×2 cm^2 Al_2O_3 substrate. After completing the two mentioned processes, we allowed natural cooling for 1 h. In figure 1, which represents the CVD schematic, you can observe various synthesized shapes

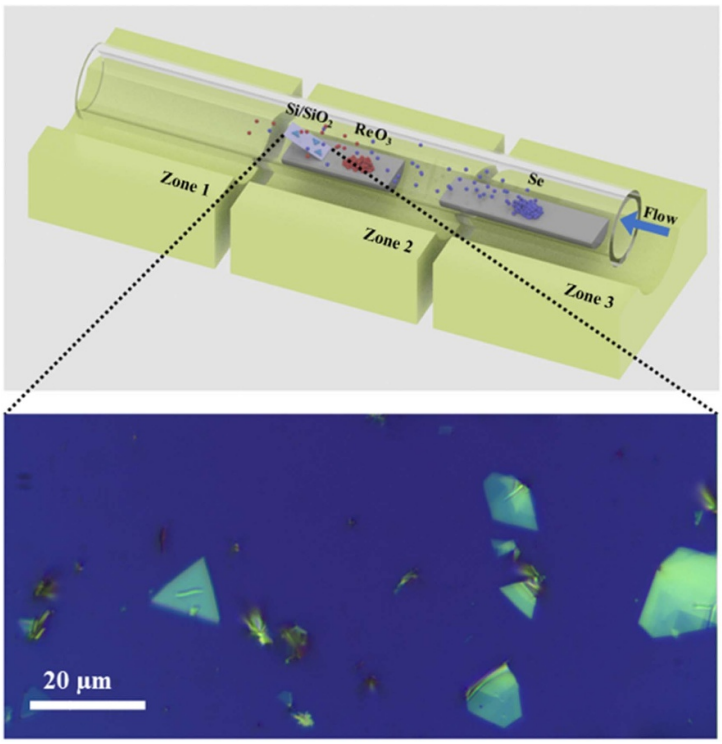

Figure 1. Schematic of the CVD growth of $ReSe_2$ in the confined reaction space and the surface reaction on Si/SiO_2.

such as triangles, diamonds, trapezoids, etc, with sizes around 21 μm. By using a tilted substrate, we reduced the boundary layer and confirmed successful synthesis. Boundary layer represents the boundary between the deposited material and the surface where the reaction occurs, occurring as the reactants move towards the surface and deposit during the process. Reducing the thickness of the boundary layer can increase the efficient transfer of reactants and the rate of deposition. The tilted substrate is placed on a boat with a length of 5 cm, with a 20-degree tilt. The distance between the tilted substrate and ReO_3 is 6 cm, while the distance between ReO_3 and Se is 9 cm. Consequently, we propose tilting as one of the methods for CVD synthesis.

2.4. Characterization

The Raman equipment used was the Raman Touch from NANO PHOTON, employing a green 532 nm laser for excitation. For FE-SEM imaging, the Carl Zeiss Gemini 500 system was utilized, along with an EsB detector, and EDS data were obtained using the EDS detector integrated into the FE-SEM. The AFM equipment used was the Multimode-8 from BRUKER. x-ray photoelectron spectroscopy (XPS) measurements were carried out using the Axis Supra+ from Kratos Analytical Ltd, with a 20 s etching applied during XPS measurements. The transmission electron microscopy (TEM) equipment used was the JEM-ARM200F with a spherical aberration corrector (Cs corrector), and TEM samples were prepared on grid using focused-ion beam techniques.

3. Result and discussion

The optical configuration for chiral Raman scattering measurements is illustrated in figure 2. A quarter-wave plate ($\theta/2$) is employed to generate either right-handed (RCP) or left-handed (LCP) circular polarization during excitation. The scattered light then traverses the same $\theta/2$ and is subsequently collected without the use of analyser.

We conducted the $ReSe_2$ film synthesis process following the recipe mentioned in the experimental details. Figure 3(a) clearly shows well-defined peaks around 125 cm^{-1}, 169 cm^{-1}, and 174 cm^{-1}, which are characteristic Raman peaks of $ReSe_2$ [10, 29, 30]. In previous processes without tilting, Raman spectra did not yield satisfactory results, lacking the detection of relatively low-intensity peaks. The boundary layer refers to the layer in which the flow of fluid near the surface of an object converges to a speed of zero as it approaches the substrate surface. This layer affects the fluid's velocity. In the absence of tilting, the flow near the object's substrate surface can be uneven due to the gas diffusion to the edge of the substrate affected by the boundary layer. This can result in non-uniform deposition or lack of deposition. Therefore, by tilting, we

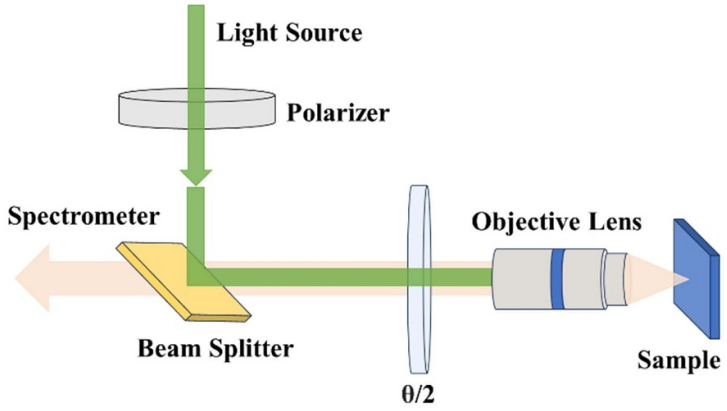

Figure 2. Optical setup of the chiral Raman scattering measurements.

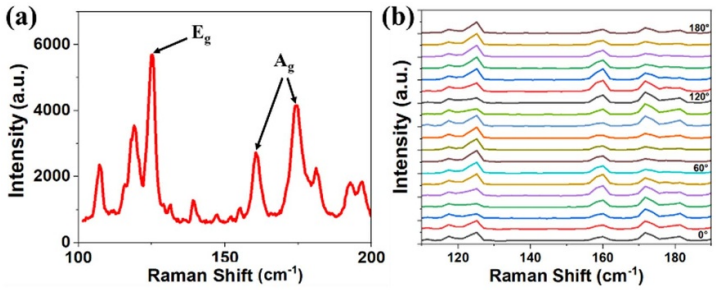

Figure 3. (a) Raman Spectra of as-grown $ReSe_2$ (b) To investigate the Raman spectra variations with incident light polarization, Raman intensity was examined at each angle from 0° to 180°.

ensure that the flow can reach the entire front surface of the substrate regardless of the boundary layer's location [31, 32]. Before confirming the anisotropic properties of $ReSe_2$ in figure 3(b), we explored changes int the Raman spectra by varying the incident light polarization angle from 0° to 180°. Raman intensity was observed at 125 cm^{-1}, 159 cm^{-1}, and 171 cm^{-1} at all angles, revealing variations in intensity with respect to the angle. To delve into these differences in detail, polarization mapping was conducted. The deposition of $ReSe_2$ was also confirmed by the color change on the surfaces of Si/SiO_2 and sapphire substrates, as shown in Figures S1 (a) and (b). Not only the continuous film, but also hexagonal and sunflower shapes could be synthesized by adjusting the recipe. The Raman peaks and intensities for each shape can be found in Figure S2. Furthermore, Figure S2 presents Raman spectra for hexagonal and sunflower-shaped $ReSe_2$ flakes. It confirms the presence of $ReSe_2$ Raman peaks with peaks near 125 cm^{-1}, 169 cm^{-1}, and 174 cm^{-1} [1]. The differences in peak intensities depending on the shape are also noticeable.

In figure 4(a), we validated the anisotropic characteristics by observing the ideal Raman spectra peak through Raman spectroscopy. These anisotropic features on a 2D plane result in energy level splitting for linearly polarized light, and the characteristics vary with the direction of the incident light, making it suitable for image sensors and optoelectronic devices [3–9]. Furthermore, in figure 4(b) $\theta_L V_R$ fitting through ARPRS was employed to provide a more intuitive representation of the anisotropic properties of $ReSe_2$ flakes. Color plots were generated to illustrate the changes in intensity with respect to angles. It was observed that the intensity is high around Raman shifts of approximately 125 cm^{-1} and 169 cm^{-1}.

Additionally, to confirm the thickness of the $ReSe_2$ growth, we conducted AFM measurements, as depicted in figure 5(a), revealing a film thickness of approximately 4 nm. Since a monolayer of $ReSe_2$ is ∼0.7 nm, we can confirm that our film consists of 5–6 layers [1, 17]. Furthermore, it is apparent that the right section of the image displays uniform deposition, providing confirmation of the existence of a continuous layer. In the initial experiments, when 100 mg of Se was used, the thickness was formed to be approximately 20–30 nm. In order to produce $ReSe_2$ films with reduced thickness, the Se qu antity was systematically decreased from 100 mg to 60 mg. This reduction was necessary because Se possesses low chemical reactivity, and precise control over both the amount of Se and the temperature is vital during the synthesis of Se-based TMDs (Se-TMDs) [33]. Typically, a larger amount of Se results in the deposition of thicker films. Since the previous $ReSe_2$ film was notably thick, we aimed to deposit as few layers as possible by

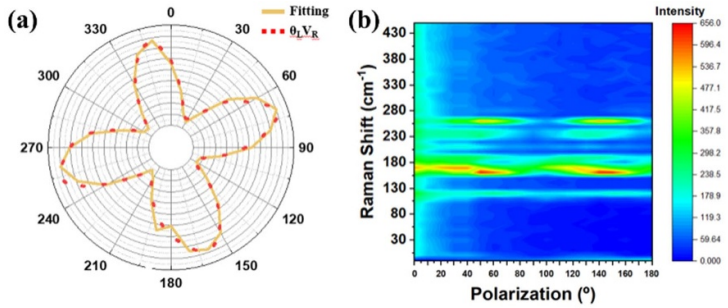

Figure 4. (a) This is a Raman intensity mapping image as a function of angle in-plane (b) color plots of angle-resolved polarized Raman spectroscopy (ARPRS) of $ReSe_2$ flakes under the $\theta_L V_R$ configuration.

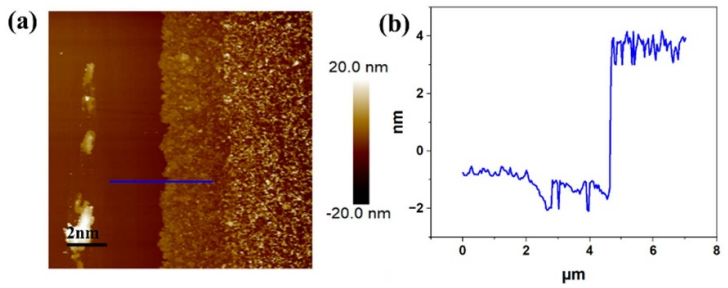

Figure 5. (a) AFM full image of film type $ReSe_2$ (b) AFM-based thickness measurement data for Film-Type $ReSe_2$.

reducing the amount of Se gradually to 60 mg. And, by using 75 sccm of Ar gas without using hydrogen, it was possible to synthesize a thinner $ReSe_2$ in flake form. The processing time was adjusted progressively from 5 min to 30 min. When processed for 5 min, the Se sample did not completely melt, and the ReO_3 sample did not undergo reduction. At temperatures exceeding 400 °C, ReO_3 initiates decomposition into Re_2O_7 (volatile) and ReO_2 (less volatile), as indicated by the following reaction, as reported in [34]:

$$3ReO_3 \rightarrow Re_2O_7 + ReO_2.$$

We controlled th at 5 min intervals, and when the experiment was conducted for less than 20 min, ReO_3 did not melt. Hence, our determination was that a minimum of 20 min of running time proved to be effective in achieving reduction and melting. The typical process of film growth entails the initiation of nuclei, which then steadily expand into successive layers. As deposition time progresses, the sample is continuously exposed to thermal energy, leading to nucleation and layer growth, which results in an increase in sample thickness. However, in the case of materials like $ReSe_2$, it was experimentally observed that desorption begins to occur after an extended period, typically exceeding 20 min. When the process was conducted for 25–30 min, no material was generated on the substrate. Consequently, we conducted the process for 20 min, at which point flakes were observed to form. Therefore, we established the recipe with a 20 min process time, just before desorption [35, 36].

We have confirmed that the growth behavior of $ReSe_2$ crystals depends on the type of growth substrates. The concentration of precursor at the growth front determines the direction of crystal growth, either out-of-plane or in-plane [37–40]. In figure 6(a), we confirmed that pyramid-shaped ReSe2 flakes grown in the out-of-plane direction on SiO_2 growth substrates with relatively many dangling bonds on the surface. On the other hand, on the Al_2O_3 growth substrate, where the precursor is relatively easy to diffuse, we observed that film-like ReSe2 was synthesized, as shown in figure 6(b) [40]. In addition, we confirmed ReSe2 of various morphologies and performed EDS mapping analysis, as shown in Figures S3 and S4. The atomic percentages reveal that the ratio of Re–Se is approximately 0.03%–0.07%, confirming the presence of Re and Se. This information can be verified in table S1. Additionally, figures S4(a) and (b) exhibit SEM images of $ReSe_2$ flakes in various shapes, distinct from the previously observed triangular shape. These images provide further verification of the deposition of various morphology of $ReSe_2$.

In figures 7(a) and (b), the XPS data for $ReSe_2$ reveal that the binding energies of Re atoms in the $4f^{7/2}$ and $4f^{5/2}$ orbitals were determined to be 40.6 eV and 46.5 eV, respectively. Moreover, the XPS analysis

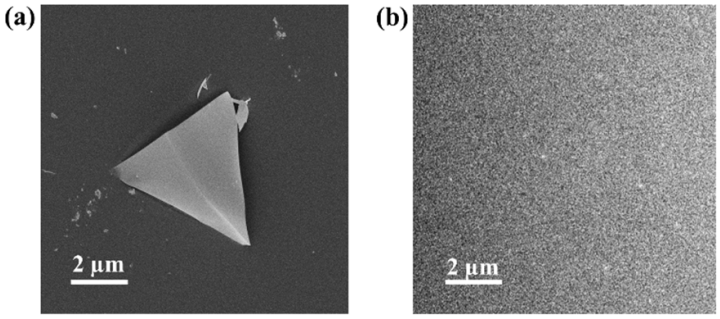

Figure 6. Characterization of the composition and structure of the CVD-grown $ReSe_2$ flake (a) SEM images of pyramid shape $ReSe_2$ grown on Si/SiO_2 the scale bar represents 2 μm. (b) SEM Image of Continuous film $ReSe_2$ on Al_2O_3. The scale bar represents 2 μm.

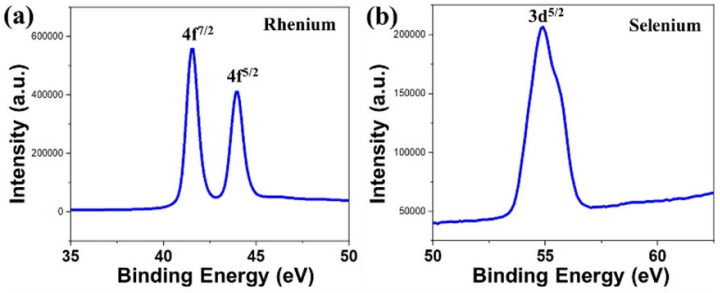

Figure 7. (a) (b) Detailed XPS Signals of Re 4*f* and Se 3*d* spectra.

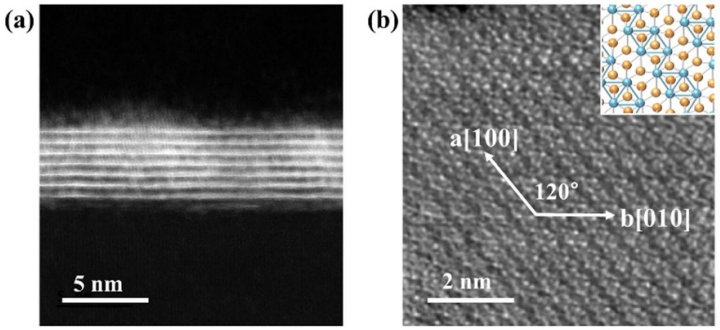

Figure 8. (a) TEM Image side view. The scale bar represents 5 nm. (b) TEM Image of atom structure. The scale bar represents 2 nm.

revealed a binding energy of 55 eV for Se atoms in the $3d^{5/2}$ orbital [29]. Additionally, the atomic ratio of Re to Se in the XPS spectra was found to be 1:2.16, providing confirmation of the stoichiometric composition of $ReSe_2$ in a 1:2 ratio. This observation signifies the production of $ReSe_2$ flakes in the MX_2 form.

In figure 8, we utilized TEM to confirm the atomic structure and determine the thickness of the $ReSe_2$ film. Figure 8(a) displays a side view of the image, revealing the atomic arrangement, which verifies the presence of seven layers bonded together by van der Waals forces. We quantified the total thickness to be approximately 4.9 nm, with each layer having a thickness of about 0.7 nm [1]. Furthermore, in figure 8(b), the atomic arrangement structure of planar $ReSe_2$, particularly the DC chain, is elucidated. The characteristic diamond chain structure of rhenium (Re) can be observed. The planes of the [100] *a*-axis and [010] *b*-axis exhibit a 120-degree difference. This alignment is consistent with the findings reported in previous studies [3–9].

4. Conclusion

In this paper, we have identified the optimal conditions for synthesizing $ReSe_2$ in both flake and film forms. We maximized the synthesis rate by using a substrate tilting boat to ensure a uniform and minimal layer formation on the substrate front, thereby controlling the boundary layer. Additionally, we optimized the crucial parameters, such as the amount of Se and the gas within the tube, to synthesize $ReSe_2$ in both flake and film forms and determined the corresponding process times. To achieve stable deposition, we reduced the amount of Se, decreased the previously used amount of Ar, eliminated H_2, and derived the desorption time after complete sample reduction, thus enhancing the $ReSe_2$ synthesis rate. Furthermore, we confirmed the $ReSe_2$ intrinsic properties, such as its anisotropic characteristics, indicating its potential for use in photo devices. We hope this paper serves as a guide for large-area synthesis of $ReSe_2$. Additionally, we believe that this material can be utilized to create a variety of spectral components by forming van der Waals heterostructures, not only for optical and electrical devices but also for applications as the next-generation semiconductor.

Data availability statement

All data that support the findings of this study are included within the article (and any supplementary files).

Acknowledgment

G. Nam, S. Park, K. Heo contributed equally to this work. This work was supported by the Basic Science Research Program and Basic Research Lab Program through the National Research Foundation of Korea (NRF) funded by the Ministry of Education (2022R1I1A307258213),(RS-2023-00221295), (2022R1C1C2004541).

Materials/Parts Technology Development Program (20022480) funded By the Ministry of Trade, Industry & Energy(MOTIE, Korea). This work was also supported by Korea Initiative for fostering University of Research and Innovation Program of the National Research Foundation (NRF) funded by the Korea government (MSIT) ((No. NRF2021M3H1A104892211).

ORCID iDs

Hagyoul Bae https://orcid.org/0000-0002-2462-4198
Hyeong Gi Park https://orcid.org/0000-0002-9590-1623
Jae-Hyun Lee https://orcid.org/0000-0001-5117-8923
Hyeon-Sik Jang https://orcid.org/0000-0002-5164-6624

References

[1] Wolverson D, Crampin S, Kazemi A S, Ilie A and Bending S J 2014 Raman spectra of monolayer, few-layer, and bulk ReSe2: an anisotropic layered semiconductor *ACS Nano* **8** 11154–64
[2] Lamfers H-J, Meetsma A, Wiegers G and De Boer J 1996 The crystal structure of some rhenium and technetium dichalcogenides *J. Alloys Compd.* **241** 34–39
[3] Li H, Zhang Q, Yap C C R, Tay B K, Edwin T H T, Olivier A and Baillargeat D 2012 From bulk to monolayer MoS_2: evolution of Raman scattering *Adv. Funct. Mater.* **22** 1385–90
[4] Perea-López N *et al* 2013 Photosensor device based on few-layered WS_2 films *Adv. Funct. Mater.* **23** 5511–7
[5] Voiry D *et al* 2013 Enhanced catalytic activity in strained chemically exfoliated WS_2 nanosheets for hydrogen evolution *Nat. Mater.* **12** 850–5
[6] Huo N, Kang J, Wei Z, Li S S, Li J and Wei S H 2014 Novel and enhanced optoelectronic performances of multilayer MoS_2–WS_2 heterostructure transistors *Adv. Funct. Mater.* **24** 7025–31
[7] Jo S, Ubrig N, Berger H, Kuzmenko A B and Morpurgo A F 2014 Mono-and bilayer WS_2 light-emitting transistors *Nano Lett.* **14** 2019–25
[8] Perea-López N *et al* 2014 CVD-grown monolayered MoS_2 as an effective photosensor operating at low-voltage *2D Mater.* **1** 011004
[9] Mao D, Wang Y, Ma C, Han L, Jiang B, Gan X, Hua S, Zhang W, Mei T and Zhao J 2015 WS_2 mode-locked ultrafast fiber laser *Sci. Rep.* **5** 7965
[10] Lorchat E, Froehlicher G and Berciaud S 2016 Splitting of interlayer shear modes and photon energy dependent anisotropic Raman response in N-layer $ReSe_2$ and ReS_2 *ACS Nano* **10** 2752–60
[11] Lin Y-C, Komsa H-P, Yeh C-H, Bjorkman T, Liang Z-Y, Ho C-H, Huang Y-S, Chiu P-W, Krasheninnikov A V and Suenaga K 2015 Single-layer ReS_2: two-dimensional semiconductor with tunable in-plane anisotropy *ACS Nano* **9** 11249–57
[12] Chenet D A, Aslan B, Huang P Y, Fan C, Van Der Zande A M, Heinz T F and Hone J C 2015 In-plane anisotropy in mono-and few-layer ReS_2 probed by Raman spectroscopy and scanning transmission electron microscopy *Nano Lett.* **15** 5667–72
[13] Pham P V, Bodepudi S C, Shehzad K, Liu Y, Xu Y, Yu B and Duan X 2022 2D heterostructures for ubiquitous electronics and optoelectronics: principles, opportunities, and challenges *Chem. Rev.* **122** 6514–613
[14] Jariwala B, Voiry D, Jindal A, Chalke B A, Bapat R, Thamizhavel A, Chhowalla M, Deshmukh M and Bhattacharya A 2016 Synthesis and characterization of ReS_2 and $ReSe_2$ layered chalcogenide single crystals *Chem. Mater.* **28** 3352–9

[15] Wang X, Huang L, Peng Y, Huo N, Wu K, Xia C, Wei Z, Tongay S and Li J 2016 Enhanced rectification, transport property and photocurrent generation of multilayer ReSe $_2$/MoS_2 p–n heterojunctions *Nano Res.* **9** 507–16
[16] Zong J-Q, Zhang S-F, W-x J, Zhang C-W, Li P and Wang P-J 2019 Strain-mediated stability of structures and electronic properties of ReS_2, Janus ReSSe, and $ReSe_2$ monolayers *J. Nanomater.* **2019** 1–8
[17] Alcock N and Kjekshus A 1965 The crystal structure of $ReSe_2$ *Acta Chem. Scand.* **19** 79
[18] Friemelt K, Akari S, Lux-Steiner M C, Schill T, Bucher E and Dransfeld K 1992 Scanning tunneling microscopy with atomic resolution on ReS_2 single crystals grown by vapor phase transport *Ann. Phys.* **504** 248–53
[19] Murray H, Kelty S, Chianelli R and Day C 1994 Structure of rhenium disulfide *Inorg. Chem.* **33** 4418–20
[20] Kelty S P, Ruppert A F, Chianelli R R, Ren J and Whangbo M-H 1994 Scanning probe microscopy study of layered dichalcogenide ReS_2 *J. Am. Chem. Soc.* **116** 7857–63
[21] Smithe K K, Suryavanshi S V, Muñoz Rojo M, Tedjarati A D and Pop E 2017 Low variability in synthetic monolayer MoS_2 devices *ACS nano* **11** 8456–63
[22] Zhu X, Li D, Liang X and Lu W D 2019 Ionic modulation and ionic coupling effects in MoS_2 devices for neuromorphic computing *Nat. Mater.* **18** 141–8
[23] Li N *et al* 2022 Gate-tunable large-scale flexible monolayer MoS_2 devices for photodetectors and optoelectronic synapses *Nano Res.* **15** 5418–24
[24] Chamlagain B *et al* 2014 Mobility improvement and temperature dependence in $MoSe_2$ field-effect transistors on parylene-C substrate *ACS Nano* **8** 5079–88
[25] Zhong F *et al* 2021 Substitutionally doped $MoSe_2$ for high-performance electronics and optoelectronics *Small* **17** 2102855
[26] Ghetiya A, Chaki S H, Khimani A J, Hirpara A B, Kannaujiya R M, Patel S and Deshpande M P 2021 Growth and characterizations of rhenium disulfide (ReS_2) single crystals *Phys. Status Solidi* A **218** 2000687
[27] Ji L-J, Qin Y, Gui D, Li W, Li Y, Li X and Lu P 2018 Quantifying the exfoliation ease level of 2D materials via mechanical anisotropy *Chem. Mater.* **30** 8732–8
[28] Gao Z-D, Jiang Z-H-Y, Li J-D, Li B-W, Long Y-Y, Li X-M, Yin J and Guo W-L 2022 Anisotropic mechanics of 2D materials *Adv. Eng. Mater.* **24** 2200519
[29] Hafeez M, Gan L, Li H, Ma Y and Zhai T 2016 Chemical vapor deposition synthesis of ultrathin hexagonal $ReSe_2$ flakes for anisotropic raman property and optoelectronic application *Adv. Mater.* **28** 8296–301
[30] Satheesh P P, Jang H-S, Pandit B, Chandramohan S and Heo K 2023 2D rhenium dichalcogenides: from fundamental properties to recent advances in photodetector technology *Adv. Funct. Mater.* **33** 2212167
[31] Dryden H L 1948 Recent advances in the mechanics of boundary layer flow *Adv. Appl. Mech.* **1** 1–40
[32] Mukhopadhyay S 2012 Analysis of boundary layer flow and heat transfer along a stretching cylinder in a porous medium *Int. Scholarly Res. Not.* 2012 704984
[33] Gao J, Li L, Tan J, Sun H, Li B, Idrobo J C, Singh C V, Lu T-M and Koratkar N 2016 Vertically oriented arrays of ReS_2 nanosheets for electrochemical energy storage and electrocatalysis *Nano Lett.* **16** 3780–7
[34] Cui F *et al* 2017 Epitaxial growth of large-area and highly crystalline anisotropic $ReSe_2$ atomic layer *Nano Res.* **10** 2732–42
[35] Bird T A, Wilkinson M G, Keen D A, Smith R I, Bristowe N C, Dove M T, Phillips A E and Senn M S 2021 Soft-mode anisotropy in the negative thermal expansion material ReO_3 *Phys. Rev.* B **104** 214102
[36] Jo J-E, Jorgensen J, Batlogg B, Remeika J and Axe J 1986 Order parameter and critical exponent for the pressure-induced phase transitions in ReO_3 *Phys. Rev.* B **33** 4793
[37] Negri M, Francaviglia L, Kaplan D, Swaminathan V, Salviati G, I Morral A F and Fabbri F 2022 Excitonic absorption and defect-related emission in three-dimensional MoS_2 pyramids *Nanoscale* **14** 1179–86
[38] Sial M N, Usman M, Zheng B, Yu Y, Mavrič A, Qing F, Valant M and Wang Z M 2018 CVD growth of molybdenum diselenide surface structures with tailored morphology *CrystEngComm* **20** 4867–74
[39] Chen L, Liu B, Abbas A N, Ma Y, Fang X, Liu Y and Zhou C 2014 Screw-dislocation-driven growth of two-dimensional few-layer and pyramid-like WSe_2 by sulfur-assisted chemical vapor deposition *ACS Nano* **8** 11543–51
[40] Li X *et al* 2016 Controlled growth of large-area anisotropic ReS_2 atomic layer and its photodetector application *Nanoscale* **8** 18956–62